BASE-ISOLATION AGAINST OUT-OF-PLANE SEISMIC DAMAGE OF MASONRY INFILLS IN EXISTING HOSPITALS

F. Mazza[1], S. Rizzuti[2]

[1] *Professor, Department of Civil Engineering, University of Calabria, fabio.mazza@unical.it*
[2] *Research fellow, Department of Civil Engineering, University of Calabria, sabrinarizzuti94@gmail.com*

Abstract

Masonry infills (MIs) are often prone to out-of-plane (OOP) collapse mechanisms during earthquakes, with devastating consequences for public buildings such as hospitals. Base-isolation systems represent one of the most effective techniques currently used for the seismic protection of structural parts and reducing the risk of the in-plane (IP) damage of MIs, but no attention has been paid in the literature to their influence on improving the OOP behaviour of these nonstructural components. To full this gap, a medical centre with a five-storey reinforced concrete (r.c.) framed structure is designed (as fixed-base) in compliance with a former Italian seismic code, for a medium-risk zone. Four infill aspect ratios (i.e. width-to-height ratio equal to 1, 1.25, 1.5 and 1.75) are examined, combining bays of different lengths with exterior (i.e. configuration C1) and interior (i.e. configuration C2) arrangements of MIs. Four structural models are considered, assuming: i) and ii), bare structures with nonstructural MIs, constructed so as to avoid affecting structural stiffness, fulfilling provisions of the former and current Italian seismic codes for limiting nonstructural damage; iii) and iv), infilled structures, with the C1 and C2 configurations of structural MIs in contact with the frame but not structurally connected, applying only provisions of the former Italian code. Then, these structures are retrofitted with a base-isolation system of high-damping-rubber bearings (HDRBs), to meet the requirements of the current Italian code in a high-risk seismic zone. The same values of the fundamental vibration period and equivalent viscous damping ratio in the horizontal direction are considered for all retrofitted structures. A five-element macro-model comprising four diagonal nonlinear beams and one (horizontal) central nonlinear truss for the prediction of OOP and IP behaviour of MIs, respectively, is implemented in a C++ computer code for the nonlinear dynamic analysis of the infilled r.c. framed structures. The proposed algorithm addresses the issue of nonlinear interaction by modifying stiffness and strength values of the MI in the OOP direction on the basis of simultaneous or prior IP damage. R.c. frame members of the superstructure are described by a lumped plasticity model, with hardening ratio equal to 3%, in which the axial load and biaxial bending moment interaction of the r.c. cross-sections is computed by a piecewise linearization of the limit surface. An advanced three-spring-three-dashpot model is adopted to take into account the observed behaviour of the HDRBs during severe earthquakes: high vertical forces significantly affect the horizontal response; softening occurs in the vertical direction with notable lateral deformations; horizontal stiffness lessens with increasing horizontal displacement; the equivalent viscous damping in the horizontal direction depends on the amplitude of displacement the bearing is subjected to and, ultimately, on the amplitude of the shear strain. Finally, bare and infilled models of the fixed-base and base-isolated hospitals are subjected to biaxial spectrum-compatible far- and near-field artificial accelerograms scaled at the level of the life-safety provided by the current Italian seismic code.

Keywords: seismic retrofitting of hospitals; in-plane and out-of-plane response of infills; r.c. framed structures; base-isolation; nonlinear seismic analysis.

1. Introduction

Since the successful base-isolation of the University of California (USC), which prevented any damage after the 1994 Northbridge earthquake, unlike the severe damage suffered by the nearby fixed-base Los Angeles County hospital complex, base-isolation applications for new hospitals have become very common worldwide [1]. Indeed, Italy can boast the first (Frosinone hospital, Lazio) and the largest (Del Mare hospital in Naples) base-isolated structures in Europe. More work is still needed, however, to demonstrate the suitability of base-isolation for such crucial public buildings, where poor seismic performance is related not only to structural failure but also to the inability of such services to ensure the continued functioning also of non-structural building elements [2]. As an example, these NSBEs represent about 44% (non-structural components) and 48% (technological contents) of the total cost of hospital construction in the USA [3]. Moreover, indirect economic losses due to the damage of NSBEs in hospital buildings is greater than the cost of structural damage, also because the former can occur at much lower seismic intensities and the downtime costs of the hospital's inability to continue working after an earthquake can be considerable [4]. NBSEs are generally classed as "acceleration-sensitivities" (e.g. suspended ceilings and piping) and "displacement-sensitivities" (e.g. masonry walls and partitions), to which "the velocity-sensitivities" class has recently been added. Yet it would be more correct to classify masonry infills (MIs) as "acceleration sensitivities" at the upper floors where the OOP drift ratio increases due to an increase in floor inertia forces, "displacement-sensitivities" at the lower floors, due to significant OOP damage from the highest values of IP drift ratio in the supporting structure, and "acceleration and displacement-sensitivities" at the intermediate floors.

One of the most dangerous aspects of the collapse of NSBEs is the OOP falling debris of MIs, which can be responsible for casualties as well as damage to critical medical equipment in the vicinity [7]. The present work is aimed to assess the seismic performance of hospital buildings retrofitted by means of base-isolation, to determine whether this type of intervention is able to preserve the hospital's ability to function. To this end, a simulated design of a medical centre with a five-storey reinforced concrete (r.c.) framed structure is carried out as fixed-base, in line with a former Italian seismic code [8], for a medium-risk zone. Four infill aspect ratios (i.e. width-to-height ratio equal to 1.0, 1.25, 1.5 and 1.75) of two equal-width leaves of hollow clay bricks are examined, combining bays of different lengths with exterior (i.e. configuration C1) and interior (i.e. configuration C2) arrangements of MIs in the perimeter frames. Four structural models are designed: i.e., bare frames with non-structural MIs fulfilling provisions of the former [8] and current [9] Italian seismic codes; infilled frames with the C1 and C2 configurations of structural MIs, applying only provisions of the former Italian code. Then, these structures are retrofitted by the insertion of a base-isolation system constituted of high-damping-rubber bearings (HDRBs), to meet the requirements of the current Italian code in a high-risk seismic zone, on the assumption that the same fundamental vibration period and equivalent viscous damping in the horizontal direction are considered for all the base-isolated structures. A five-element macro-model of MIs, proposed in a previous work [10] and implemented in a C++ computer code for the nonlinear dynamic analysis of r.c. spatial framed structures [11], is adopted to predict the interaction between in-plane and out-of-plane behaviour of masonry infills. Based on a piecewise linearization of the axial load-biaxial bending moment elastic domain, a lumped plasticity model is used to describe the inelastic behaviour of the r.c. frame members [12] while a three-spring-three-dashpot model is adopted to take into account the nonlinear behaviour of the HDRBs [13]. Finally, nonlinear seismic analysis of the bare and infilled models of the fixed-base and base-isolated hospitals are subjected to biaxial spectrum-compatible far-fault and near-fault artificial accelerograms [14] scaled at the life-safety level provided by current Italian seismic code for risk category IV.

2. Layout, design and retrofitting of the hospital buildings

Hospital composed of a reinforced concrete (r.c.) five-storey framed structure with constant storey height and bays of different length along the in-plan X and Y principal directions is chosen as test structure for the numerical investigation (Fig. 1). Four infill aspect ratios (i.e. width-to-height ratio L/h equal to 1, 1.25, 1.5 and 1.75) are examined, considering exterior (i.e. configuration C1, Figs. 1b,c) and interior (i.e.

configuration C2, Figs. 1d,e) arrangements of MIs. Deep beams are placed around the perimeter while interior deep and flat beams are placed perpendicular and parallel to the floor slab direction, respectively; all perimeter columns have a rectangular cross-section oriented as shown in Fig. 1a, while all interior columns have a square cross-section. A simulated design of the original framed building is carried out in compliance with a previous Italian code (DM96, [8]), assuming: medium-risk seismic zone (seismic coefficient, C=0.07), typical subsoil class (foundation coefficient, ε=1) and strategic function after an earthquake (i.e. seismic protection coefficient, I=1.4). Four structural designs of the existing hospital in the fixed-base hypothesis are considered, complying with the ultimate limit states. Specifically, two bare frames (BFs), with nonstructural MIs constructed so as to avoid affecting structural stiffness, are designed in order to fulfill the in-plane (IP) drift ratio thresholds (i.e. Δ/h, with Δ interstorey drift and h storey height) imposed by DM96 [8] ((Δ/h)$^{(IP)}$=0.4%, BF.D1) and DM18 [9] ((Δ/h)$^{(IP)}$=0.5%, BF.D2) Italian seismic codes for limiting nonstructural damage at the serviceability limit state. Moreover, two other infilled frames (IFs), with the C1 (Figs. 1b,c) and C2 (Figs. 1d,e) configurations of structural MIs in contact with the frame but not structurally connected, are designed in line with provisions of the former Italian code [8] for a different serviceability limit state ((Δ/h)$^{(IP)}$=0.2%, IFC1.D3 and IFC2.D3). The vertical loads are represented by a dead load of 5.93 kN/m^2 on the top floor and 7.23 kN/m^2 on the other floors and a live load of 2 kN/m^2 on the top floor and 3 kN/m^2 on the other floors. Non-structural MIs are taken into account through an additional dead load of 5.5 kN/m along the perimeter beams. Concrete cylindrical compressive strength of 25 N/mm^2 and steel reinforcement with yield strength of 450 N/mm^2 are considered.

(a) Plan   (b) Elevation MI.C1 (X-Z)   (c) Elevation MI.C1 (Y-Z)

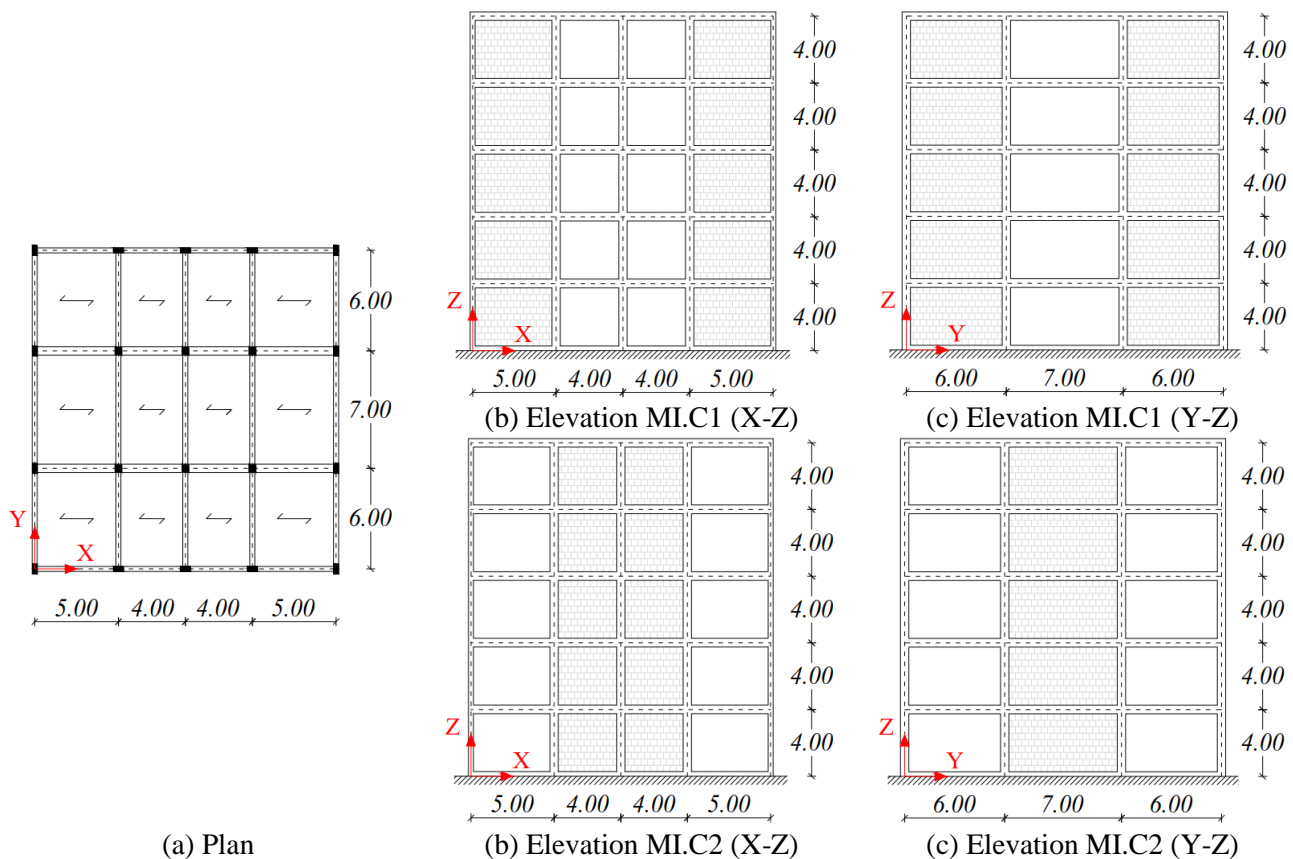(b) Elevation MI.C2 (X-Z)   (c) Elevation MI.C2 (Y-Z)

Fig. 1 – Layout of the hospital structure (unit in m): masonry infill configurations C1 (b, c) and C2 (d, e)

The geometric dimensions of the deep and flat beams and exterior and interior columns of the BF.D1, BF.D2, IFC1.D3 and IFC2.D3 structures are reported in Table 1. It is interesting to note that considerable differences of r.c. structural members are obtained for the hospital buildings, confirming that they are markedly affected by the stiffness requirements imposed by a former Italian code [8], with the highest

3

dimensions when $(\Delta/h)^{(IP)}=0.2\%$ is imposed. Dynamic properties of the four main vibration modes for bare and infilled structures, two for each principal in-plan direction, are reported in Table 2 together with the total mass of the building (m_{tot}): i.e. vibration periods (T_{iX} and T_{iY}, i=1,2); translational effective mass (m_{iX} and m_{iY}, i=1,2), expressed as a percentage of m_{tot}. Detailing for local ductility is also imposed to satisfy minimum conditions for the longitudinal bars of the r.c. frame members: for the beams, a tension reinforcement ratio nowhere less than 0.37% is provided and a compression reinforcement not less than half of the tension reinforcement is placed at all sections; for a section of each column a minimum steel geometric ratio of 1% is selected on the assumption that the minimum reinforcement ratio corresponding to one side of the section be about 0.35%. As shown the vibration periods of the IFC1.D3 and IFC2.D3 infilled structures are lower than those obtained for the BF.D1 and BF.D2 structures because an elastic strut model is also considered for MIs.

Table 1 – Geometric properties of r.c. frame members of the hospital structures (unit in m):

Structure	Storey	Deep beams	Flat beams	Perimeter columns	Interior columns
BF.D1		0.30×0.70	0.50×0.25	0.30×0.60	0.40×0.40
BF.D2	5	0.30×0.50	0.50×0.25	0.30×0.50	0.30×0.30
IFC1.D3 / IFC2.D3		0.40×0.90	0.60×0.25	0.40×0.70	0.50×0.50
BF.D1		0.30×0.75	0.50×0.25	0.30×0.70	0.50×0.50
BF.D2	4	0.30×0.55	0.50×0.25	0.30×0.60	0.40×0.40
IFC1.D3 / IFC2.D3		0.40×0.95	0.60×0.25	0.40×0.80	0.60×0.60
BF.D1		0.30×0.80	0.60×0.25	0.30×0.80	0.60×0.60
BF.D2	3	0.30×0.60	0.60×0.25	0.30×0.70	0.50×0.50
IFC1.D3 / IFC2.D3		0.40×1.00	0.70×0.25	0.40×0.90	0.70×0.70
BF.D1		0.30×0.85	0.60×0.25	0.30×0.90	0.70×0.70
BF.D2	2	0.30×0.65	0.60×0.25	0.30×0.80	0.60×0.60
IFC1.D3 / IFC2.D3		0.40×1.05	0.70×0.25	0.40×1.00	0.80×0.80
BF.D1		0.30×0.90	0.70×0.25	0.40×0.90	0.70×0.70
BF.D2	1	0.40×0.70	0.70×0.25	0.40×0.80	0.60×0.60
IFC1.D3 / IFC2.D3		0.40×1.10	0.80×0.25	0.40×1.10	0.80×0.80

Table 2 – Dynamic properties of the hospital structures (units in t, m and s)

Structure	m_{tot}	T_{1X}	m_{1X} [%m_{tot}]	T_{1Y}	m_{1Y} [%m_{tot}]	T_{2X}	m_{2X} [%m_{tot}]	T_{2Y}	m_{2Y} [%m_{tot}]
BF.D1	2369	0.677	75.25	0.574	74.56	0.250	13.77	0.219	14.55
BF.D2	2214	0.845	73.81	0.777	71.93	0.318	14.05	0.301	15.24
IFC1.D3	2773	0.488	79.00	0.408	78.92	0.176	12.51	0.151	13.10
IFC2.D3	2773	0.494	78.69	0.413	79.04	0.178	12.68	0.154	12.97

4

Next, base-isolation with elastomeric bearings is considered to retrofit the original fixed-base hospital buildings, to attain performance levels imposed by DM18 [9] in a high-risk seismic zone (i.e. peak ground acceleration on rock, a_g=0.499g at the collapse prevention (CP) ultimate limit state) and for moderately-soft subsoil (i.e. class C, site amplification factor S=1), assuming for the building a life expectancy of 100 years and usage class IV. Moreover, different live loads are considered on the floor levels, as function of their destination [9]: i.e. 5 kN/m^2 at the ground level, as emergency area; 3 kN/m^2 at the first and second levels, for medical rooms; 2 kN/m^2 at the third and fourth levels, for hospital rooms and on the roof. An additional mass of about 610, 603 and 620 t for the BF.D1, BF.D2 and IF.D3 structures, respectively, is assumed at the level of the rigid beams placed above the isolators.

The design of the elastomeric (i.e. high-damping-rubber bearings, HDRBs) base-isolation system is carried out on the assumption that the same value of the equivalent viscous damping ratios in the horizontal (ξ_H=15%) and vertical (ξ_V=5%) directions are assumed for the BI.D1, BI.D2, BIC1.D3 and BIC2.D3 base-isolated structures. Moreover, a fundamental vibration period (T_I) equal to 2.9 s is assumed for all structures, satisfying the condition $T_{BI,X} \equiv T_{BI,Y} \geq \max(3T_{FB,X}, 3T_{FB,Y})$, $T_{FB,X}$ and $T_{FB,Y}$ being the fundamental vibration periods of the same structures on fixed-base. A nominal stiffness ratio α_{K0}, defined as the ratio between the nominal value of the vertical stiffness (K_{V0}) and the analogous value of the horizontal stiffness (K_{H0}), equal to 1600 is assumed for all the isolators, considering a volumetric compression modulus of the rubber (i.e. E_b) equal to 2000 MPa and a shear modulus G= 0.40 MPa. The following geometric properties of the HDRBs are reported in Table 3: diameter of the steel layer (D_s) and that of the elastomer (D_e); thickness (t_s) of the interior steel shims; number (n_e) and thickness (t_i) of the single layer of elastomer; total thickness (t_e) of the elastomer; primary $S_1(=D_s/(4t_i))$ and secondary $S_2(=D_s/t_e)$ shape factors; displacement at the CP limit state (d_{dC}). The HDRBs fulfil the CP limit state verifications regarding the maximum shear strains (see Table 3): i.e. $\gamma_{tot} \leq 5$ and $\gamma_s \leq 2$, where γ_{tot} and γ_s represent the total design shear strain and the shear strain of the elastomer due to seismic displacement. Moreover, the maximum compression axial load (P_{max}) does not exceed the critical load (P_{cr}) divided by a safety coefficient equal to 2.0, while no tensile stress emerges from the seismic analysis. Finally, the maximum normal stress of the interior steel shims ($\sigma_{s,max}$) is less than the corresponding yielding value (σ_{sy}=2350 MPa).

Table 3 – Geometric properties and results of verifications of the base-isolation systems (unit in mm)

Structure	D_s	D_e	t_s	n_e	t_i	t_e	S_1	S_2	d_{dC}	γ_s	γ_{tot}	P_{cr}/P_{max}	$\sigma_{sy}/\sigma_{s,max}$
BI.D1	700	720	2.1	30	7.4	222	23.48	3.15	341	1.82	4.27	3.05	1.50
BI.D2	660	680	2.1	30	6.9	207	23.72	3.19	341	1.94	4.84	2.68	1.43
BIC1.D3 / BIC2.D3	760	780	2.1	30	7.9	237	23.19	3.21	341	1.75	3.79	3.69	1.75

3. Masonry infills

Masonry infills of the test structures described in Section 2 are made up of two 12 cm thick leaves in full contact with the surrounding frame, consisting of horizontally hollowed brick units divided by an intermediate 6 cm cavity. Main mechanical properties of the MIs are reported in Table 4, where: f_{wh} and f_{wv} are the compression strengths in the horizontal and vertical directions; f_{wu} is the sliding shear resistance of the mortar joints; f_{ws} is the shear resistance under diagonal compression; E_{wh} and E_{wv} are the secant moduli of elasticity in the horizontal and vertical directions; G_w is the shear modulus; ν is the Poisson coefficient.

Table 4 – Mechanical properties for masonry infills of the test structures (unit in MPa)

f_{wh}	f_{wv}	f_{wu}	f_{ws}	E_{wh}	E_{wv}	G_w	ν
1.11	1.5	0.25	0.31	991	1873	1089	0.25

5

3.1 In-plane behaviour

The IP nonlinear modelling of a MI panel with thickness t_w is represented by one (horizontal) truss element of a five-element model [10], linked to four axially rigid diagonals, of length d_w and inclined at angle θ with respect to the horizontal direction, by two cylindrical hinges allowing IP rotations but restraining OOP ones (Fig. 3a). The IP hysteretic response is represented in terms of compressive and tensile axial forces in the central element. A distributed mass for unit length ($\mu^{(IP)}$) is added to the floor mass of the beam supporting the MI. The lower bound estimation of the IP equivalent width of the MI proposed by Mainstone is employed [15]

$$b_w / d_w = 0.175 \cdot (\lambda \cdot h)^{-0.4} \tag{1}$$

h being the centreline height of a frame storey, and λ a dimensionless relative stiffness parameter introduced to characterise the column-infill contact length. The backbone curve of the lateral force-storey drift (F^{IP}-Δ^{IP}) consists of three linear branches, corresponding to the uncracked phase ($F^{IP} \leq F_1^{IP}$), the post cracking phase ($F_1^{IP} < F^{IP} \leq F_2^{IP}$) and the post-peak strength deterioration ($F_2^{IP} < F^{IP} \leq F_3^{IP}$) up to a conventional collapse point

$$F_1^{IP} = 0.4 \cdot F_2^{IP}; \quad F_2^{IP} = \sigma_{w,min} \cdot 2 t_w \cdot b_w \cdot \cos \theta; \quad F_3^{IP} = 0.7 \cdot F_2^{IP} \tag{2a,b,c}$$

being

$$\sigma_{w,min} = \min \left(\sigma_{w,1}, \sigma_{w,2}, \sigma_{w,3}, \sigma_{w,4} \right) \tag{3}$$

the lateral strength of the strut evaluated considering four IP failure modes proposed by Bertoldi et al. [16]: i.e. equivalent compressive strengths for diagonal compression (σ_{w1}), crushing in the corners in contact with the frame (σ_{w2}), sliding shear along horizontal joints (σ_{w3}) and diagonal tension (σ_{w4}). The corresponding values of stiffness are

$$k_{w1}^{IP} = \frac{E_{w\theta} \cdot b_w \cdot 2 t_w}{d_w}; \quad k_{w2}^{IP} = 0.15 \cdot K_{w1}^{IP}; \quad k_{w3}^{IP} = \frac{F_2^{IP} - F_3^{IP}}{\Delta_3^{IP} - \Delta_2^{IP}} \tag{4a,b,c}$$

where $E_{w\theta}$ represents the diagonal elastic modulus, while the displacements are:

$$\Delta_1^{IP} = \frac{F_1^{IP}}{K_{w1}^{IP}} \cdot \frac{1}{\cos^2 \theta}; \quad \Delta_2^{IP} = \Delta_1^{IP} + \frac{F_2^{IP} - F_1^{IP}}{K_{w2}^{IP}} \cdot \frac{1}{\cos^2 \theta}; \quad \Delta_3^{IP} = 50 \cdot \ln \left(\frac{F_2^{IP}}{F_3^{IP}} \cdot e^{0.02 \cdot \Delta_2^{IP} \cdot \cos \theta} \right) \cdot \frac{1}{\cos \theta} \tag{5a,b,c}$$

For the sake of brevity, the IP backbone curves corresponding to the MI.C1 and MI.C2 configurations are plotted in Fig. 3b only with reference to the first storey of the IF.D3 structure.
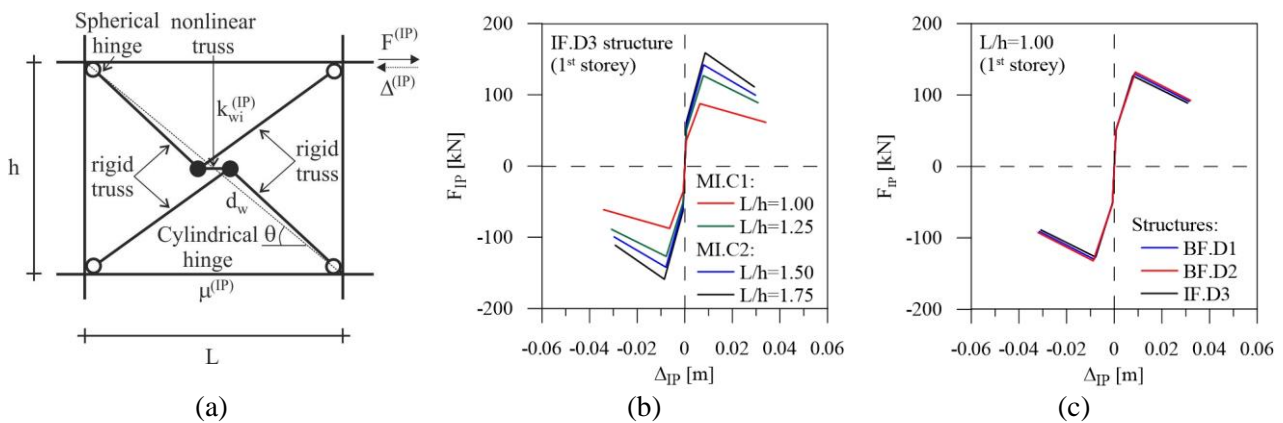

Fig. 3 – In-plane (IP) behaviour: (a) nonlinear modelling; (b) effects of width-to-height aspect ratio of MIs; (c) effects of different dimensions of the framed structure

6

It can be observed that curves related to increasing values of the infill aspect ratio are characterized by increasing values of both stiffness, for each branch, and strength, related to the points corresponding to cracking, full cracking and residual strength, but slightly decreasing ductility capacity. On the other hand, similar monotonic backbone curves are obtained for MIs at the first storey of the BF.D1, BF.D2 and IF.D3 structures, when L/h=1.0 is assumed (Fig. 3c).

3.2 Out-of-plane behaviour

The OOP nonlinear modelling of a MI panel is represented by four diagonal beams of a five-element model [10], linked to the central OOP rigid beam and to the connection joints with the frame where spherical hinges are placed in order to allow OOP rotations (Fig. 4a). The OOP hysteretic response is represented in terms of bending moment and shear force in the diagonal elements. Two masses are applied in the two central nodes (i.e. $0.5m^{(OOP)}=0.405m_{MI,tot}$, $m_{MI,tot}$ being the total mass of the panel), on the assumption that the OOP model has the same fundamental vibration period as the original MI considered as a simply supported vertical beam. The uniform OOP lateral load capacity of a MI supported on four sides, expressed in kPa, proposed by Dawe and Seah is used [17]

$$q_u =4.5 \cdot \left(f_{wv}\right)^{0.75} \cdot t_w^2 \cdot \left[\frac{\alpha}{\left(l_w\right)^{2.5}} + \frac{\beta}{\left(h_w\right)^{2.5}} \right] \tag{6}$$

where l_w and h_w are the infill height and width, expressed in mm, while the parameters α and β represent a measure of the flexural and torsional stiffnesses of the bounding columns and beams, respectively

$$\alpha = \frac{1}{h_w} \cdot \left(E_c \cdot I_{col} \cdot h_w^2 + G_c \cdot J_{t,col} \cdot t_w \cdot h_w\right)^{0.25} \le 50; \quad \beta = \frac{1}{l_w} \cdot \left(E_c \cdot I_{beam} \cdot l_w^2 + G_c \cdot J_{t,beam} \cdot t_w \cdot l_w\right)^{0.25} \le 50 \tag{7a,b}$$

being: E_c and G_c the Young and shear moduli of concrete expressed in kPa; $I_{col}(I_{beam})$ and $J_{t,col}(J_{t,beam})$ the moment of inertia and torsional constant of the column (beam), expressed in mm^4.

The backbone curve of the transversal force-storey drift ($F^{(OOP)}$-$\Delta^{(OOP)}$) considers two linear branches. In particular, the first branch represents the cracked stage until the maximum OOP resistance ($F^{OOP} \le F_1^{OOP}$), corresponding to the full arching action of the infill, and the second branch describes the post-peak strength degradation when the arching action appears to be diminishing ($F_1^{OOP} < F^{OOP} \le F_2^{OOP}$)

$$F_1^{OOP} = q_u \cdot l_w \cdot h_w; \quad F_2^{OOP} = 0.7 \cdot F_1^{OOP} \tag{8a,b}$$

The corresponding values of stiffness are

$$K_{w1}^{OOP} = E_{eq} \cdot I_{eq}; \quad K_{w2}^{OOP} = \frac{F_1^{OOP} - F_2^{OOP}}{\Delta_2^{OOP} - \Delta_1^{OOP}} \tag{9a,b,c}$$

where the moment of inertia (I_{eq}) is derived from the equivalence proposed by Kadysiewski and Mosalam between lumped masses and vibration frequency of the model [18], while the equivalent elastic modulus is obtained by imposing the equivalence of the stiffness between simply supported bi-diagonal beams and plate [10]. Finally, the OOP displacements, expressed in m, are evaluated as

$$\Delta_1^{OOP} = \frac{F_1^{OOP}}{K_{w1}^{OOP}}; \quad \Delta_2^{OOP} = \Delta_1^{OOP} + 0.02 \tag{10a,b}$$

OOP backbone curves obtained assuming different values of the in-plan aspect ratio (i.e. L/h=1.0, 1.25, 1.50 and 1.75) are shown in Fig. 4b, with reference to MIs at the first storey of the IF.D3 test structure. Note that the highest values of the forces and displacements representative of full arching action and residual strength points are those corresponding to L/h=1.75, while the lowest value of initial stiffness corresponds to L/h=1.0. Negligible influence of the dimensions of r.c. frame members is confirmed in Fig. 4c.
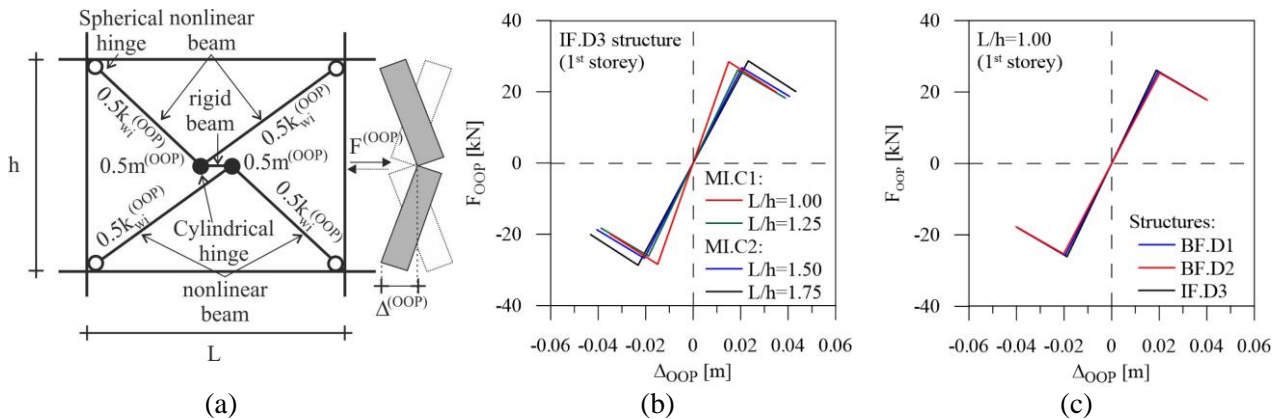
7

Fig. 4 – Out-of-plane (OOP) behaviour: (a) nonlinear modelling; (b) effects of width-to-height ratios of MIs; (c) effects of different dimensions of the framed structure

4. Numerical results

The performance of the base-isolation system with HDRBs as a seismic retrofitting solution able to avoid the OOP collapse of MIs is investigated herein with reference to hospital buildings, in order to assess their operability in the immediate aftermath of a severe earthquake. A computer code proposed in a previous work [11] is adopted to evaluate the effects of the pre- and concurrent IP damage of MIs on the reduction of the OOP strength and stiffness. OOP damage starts as soon as the IP drift ratio exceeds the thresholds corresponding to the attainment of the maximum IP strength, while the effects of OOP damage on IP behaviour are not considered [10]. A three-spring-three-dashpot viscoelastic model is adopted for an HDRB, consisting of [13]: coupled nonlinear elastic springs in the horizontal and vertical directions, with the horizontal stiffness depending on shear deformation and axial load and the vertical stiffness decreasing with increasing lateral deformation and second order geometric effects; uncoupled damping axial forces, taking into consideration that the equivalent viscous damping in the horizontal direction depends on the shear strain. Moreover, a lumped plasticity model describes the inelastic behaviour of r.c. frame members, including a 26-flat surface modelling of the axial load-biaxial bending moment elastic domain at the end sections where inelastic deformations are expected. The computer code SeismoArtif [14] is used for the generation of far-fault (inter-plate) and near-fault artificial earthquakes. The acceleration (elastic) response spectra of the artificial motions match the design spectrum adopted by DM18 [9] for the life-safety limit state and subsoil class C, assuming a range of vibration periods which contains the prescribed lower ($T_{min}=0.15s$) and upper ($T_{max}=2T_1$ and $T_{max}=1.2T_1$, where T_1 is the fundamental vibration period of the fixed-base and base-isolated structures, respectively) bound limits. Nonlinear dynamic analysis of the hospitals is carried out by means of biaxial accelerograms oriented in parallel to the principal axes of the building plan.

First, maximum values of the IP drift ratio of the framed structure, defined as drift ($\Delta_{max,IP}$) normalized by the storey height (h), and OOP drift ratio of the MIs, defined as drift ($\Delta_{max,OOP}$) normalized by half of the infill height ($h_w/2$), are shown with reference to far-fault (Fig. 5) and near-fault (Fig. 6) earthquakes (EQs). At each storey, $\Delta_{max,IP}$ and $\Delta_{max,OOP}$ are evaluated with reference to the minimum instant of time between that corresponding to the IP and OOP collapses of MIs and the final instant of simulation in the case of no collapse. Curves correspond to the following original fixed-base and retrofitted base-isolated hospitals: bare structures with non-structural MIs satisfying DM96 (i.e. BF.D1 and BI.D1) and DM18 (i.e. BF.D2 and BI.D2) provisions at the serviceability limit state; infilled structures with structural MIs of the C1 configuration taken into account with the equivalent strut approach proposed by DM96 (i.e. IF.D3 and BI.D3). As confirmed by the vibration periods reported in Table 2, MIs placed along the X axis (Figs. 5a and 6a) undergo an IP deformation greater than those on the Y axis (Figs. 5b and 6b). As can be observed, all design approaches are unable to avoid exceeding the DM96 and DM18 thresholds for the IP drift ratio of the fixed-base structures (Figs. 5a,b and 6a,b), with maximum reduction of deformability for the BF.D3.
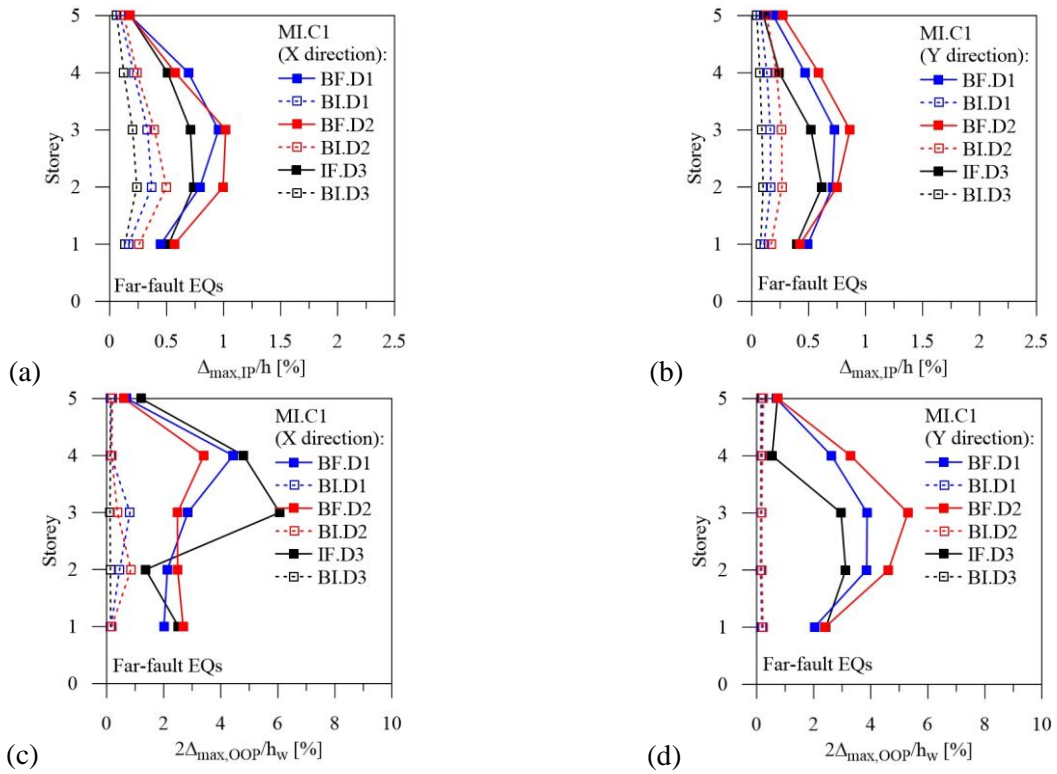
Fig. 5 – Maximum IP and OOP drifts of the hospital structures subjected to far-fault earthquakes: comparison of different design solutions for fixed-base and base-isolated structures
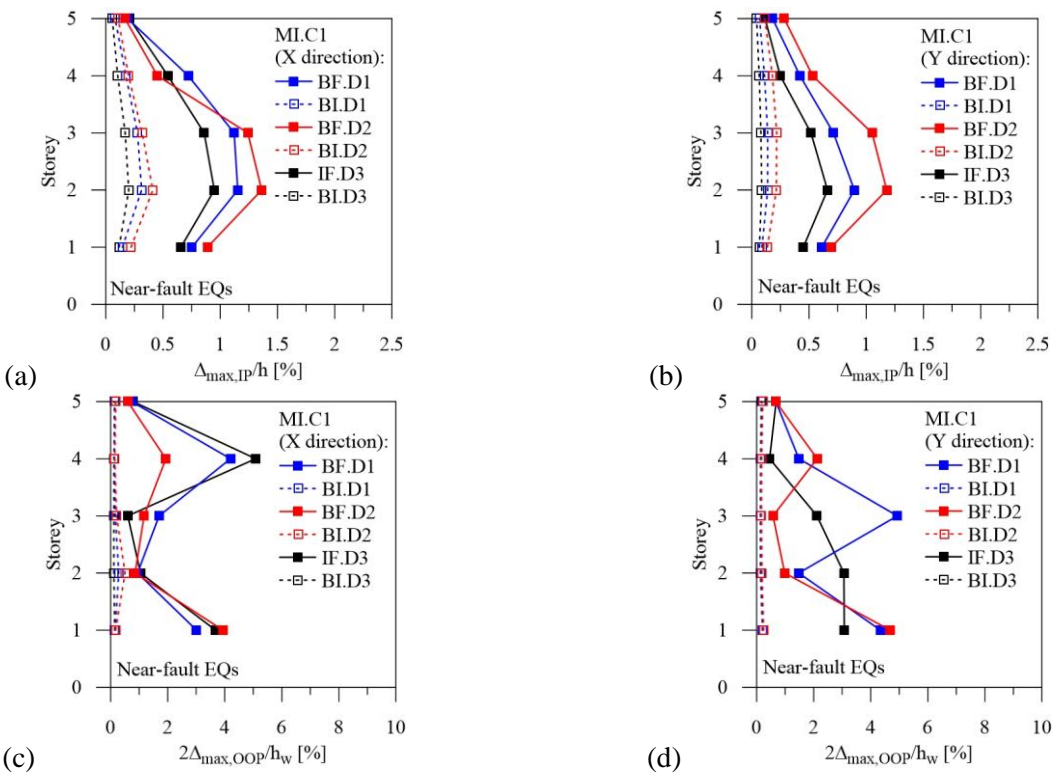

Fig. 6 – Maximum IP and OOP drifts of the hospital structures subjected to near-fault earthquakes: comparison of different design solutions for fixed-base and base-isolated structures

9

On the other hand, a notable reduction of the IP drift ratio with beneficial effects on the OOP response of MIs is observed for the base isolated structures, which always comply with the IP design thresholds.

Plots similar are shown in Fig. 7, where effects of the aspect ratio (i.e. L/h) variability of MIs are investigated with reference to the IP (Figs. 7a,c) and OOP (Figs. 7b,d) drift ratios. The focus is on the design approaches D1 (Figs. 7a,b) and D3 (Figs. 7c,d) provided by DM96 [8], with MIs placed in the C1 (i.e. L/h=1.25 and 1.5) and C2 (i.e. L/h=1 and 1.75) configurations. Note that the IP drift ratio of the fixed-base and base-isolated structures subjected to far-fault EQs generally decreases for increasing values of the aspect ratio and both design procedures (Figs. 7a,c); this is the case because the IP stiffness and strength values increase with the dimensions of the infill panel (see Fig. 3b). On the other hand, the OOP drift ratio curves corresponding to different values of L/h are crossed along the building height (Figs. 7b,d), with the highest drifts combined to the lowest L/h values at the upper storeys and vice versa at the lower ones. This is a result of two opposing effects influencing the OOP inertia forces acting on MIs: i.e. the simultaneous increase of mass and decrease of OOP acceleration for increasing values of L/h. Negligible influence of the aspect ratio on the OOP drift ratio is observed for the base-isolated structures.
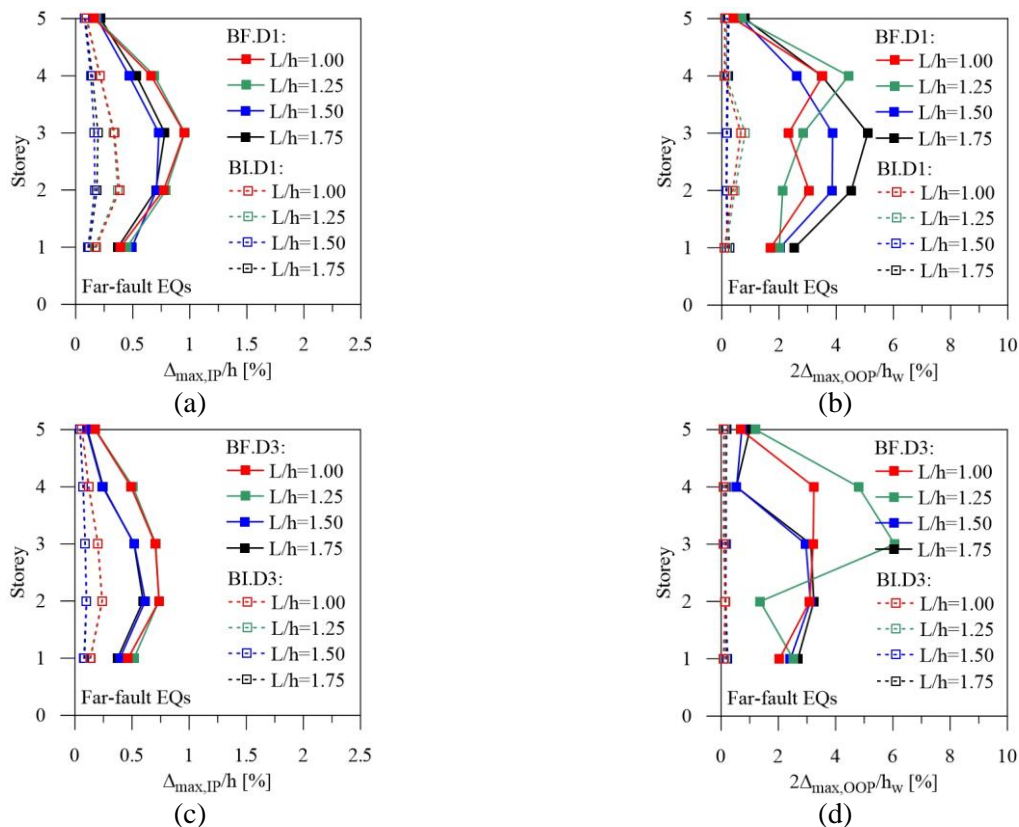

Fig. 7 – Maximum IP and OOP drifts of the hospital structures subjected to far-fault earthquakes: comparison of different infill aspect ratios for fixed-base and base-isolated structures

Finally, an overview of masonry infill panels collapsed in facades of the BF.D1, BF.D2 and IF.D3 original fixed-base structures is reported in Figs. 8 (far-fault EQ) and 9 (near-fault EQ). As shown, neither of the design procedures used in the DM96 [8] for bare and infilled structures is able to prevent the IP collapse mechanism (see red box) on the second and third levels. Moreover, OOP collapses of MIs (see blue box), that were completely disregarded in DM96, are also observed to the first four levels, in greater numbers in the case of far-fault EQ (Fig. 8) and for MIs placed in the corner bays (see C1 configuration in Figs. 8a,c,e) rather than in the central ones (see C2 configuration in Figs. 8b,d,f). Further results, omitted for brevity, have confirmed that all retrofitted base-isolated structures have been shown to be effective for the seismic protection of MIs thereby reducing the IP vulnerability and the associated OOP collapse.
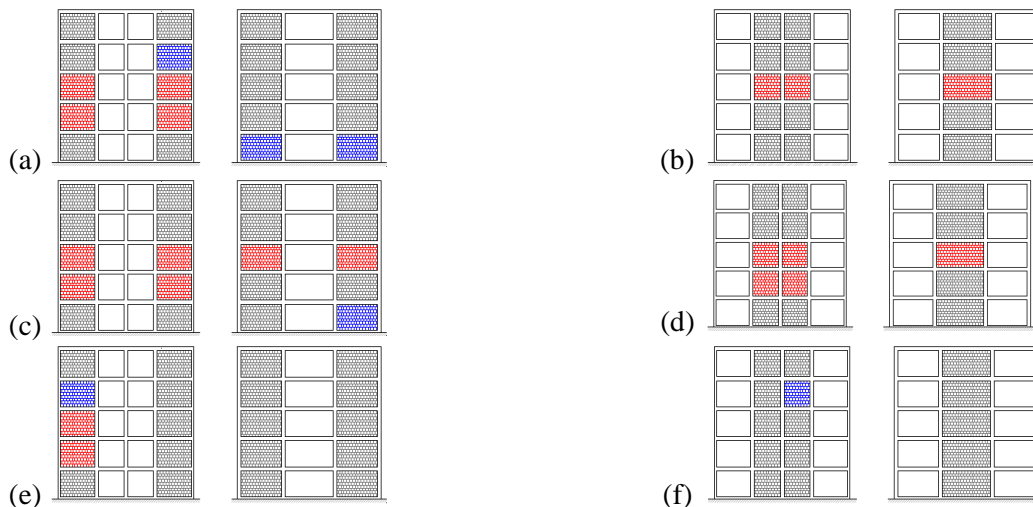
10

Fig. 8 – IP (red) and OOP (blue) collapses of MIs for fixed-base structures under far-fault earthquakes:
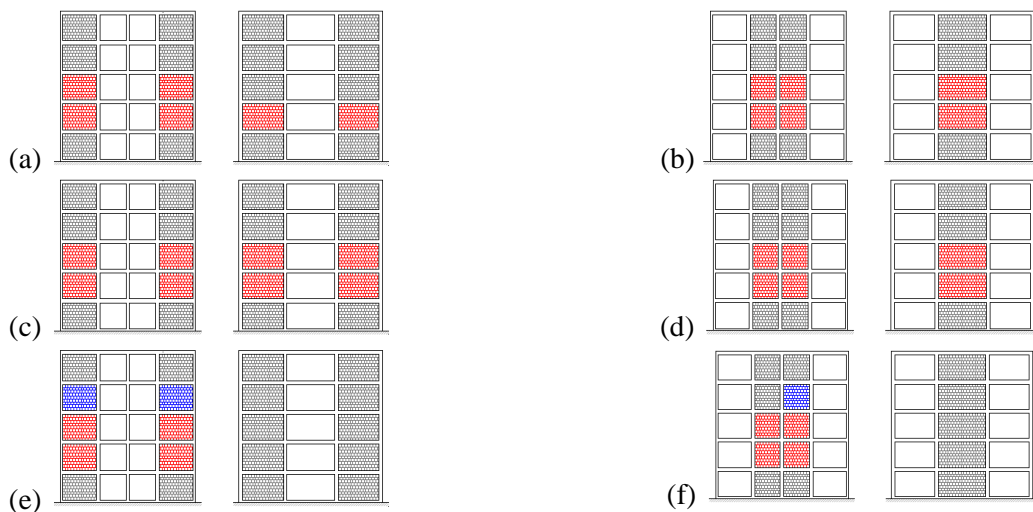(a) and (b): BF.D1; (c) and (d), BF.D2; (e) and (f), IF.D3

Fig. 9 – IP (red) and OOP (blue) collapses of MIs for fixed-base structures under near-fault earthquakes:
(a) and (b): BF.D1; (c) and (d), BF.D2; (e) and (f), IF.D3

5. Conclusions

The problem of the seismic protection of masonry infills against OOP collapse is investigated with reference to hospitals retrofitted by means of a base-isolation system, considering different design approaches of the original fixed-base structure that include the hypotheses of bare and infilled frames. Effects of corner and central configurations of MIs along the perimeter frames and four aspect ratios are also investigated. Nonlinear dynamic analyses are carried out with a ad hoc computer code, based on an IP-OOP five-element model of MIs accounting for the effects of IP damage on the OOP behaviour. Unfortunately, all the design approaches have been found to be insufficient to avoid exceeding the DM96 and DM18 thresholds for the IP drift ratio of the fixed base-structures. IP collapse mechanism occurs at the second and third levels, while OOP collapse generally affects MIs placed in the corner bays rather than in the central ones. As hoped, a notable reduction of the IP drift ratio is recorded, with beneficial effects on the OOP response of MIs, for all the base isolated structures, which always comply with the IP design thresholds without OOP collapse of MIs. Note that the IP drift ratio of the fixed-base structures generally decreases for increasing values of the aspect ratio of MIs, while maximum values of the OOP drift are observed at the upper storeys when the lowest values of the aspect ratio are considered.

11

6. Acknowledgements

7. References

[1] Erdik M, Ülker Ö, Şadan B, Tüzün C (2018): Seismic isolation code developments and significant applications in Turkey. *Soil Dynamics and Earthquake Engineering,* **115**, 413-437.

[2] Achour N, Miyajima M, Kitaura M, Price A (2011): Earthquake-induced structural and nonstructural damage in hospitals. *Earthquake Spectra,* **27** (3), 617-634.

[3] Taghavi S, Miranda E (2003): Response of nonstructural building elements. *Technical Report PEER 2003/05*, Pacific Earthquake Engineering Research Center, Berkeley, USA.

[4] Masi A, Santarsiero G, Gallipoli MR, Mucciarelli M, Manfredi V, Dusi A, Stabile TA (2013): Performance of the health facilities during the 2012 Emilia (Italy) earthquake and analysis of the Mirandola hospital case study. *Bulletin of Earthquake Engineering,* **12** (5), 2419-2443.

[5] FEMA (1999): Earthquake Loss Estimation Methodology Hazus99. *Technical Manual SR2*, Federal Emergency Management Agency, Washington, USA.

[6] Petrone C, Di Sarno L, Magliulo G, Cosenza E (2016): Numerical modelling and fragility assessment of typical freestanding building contents. *Bulletin of Earthquake Engineering*, **15** (4), 1609-1633.

[7] Braga F, Manfredi V, Masi A, Salvatori A, Vona M (2011): Performance of non-structural elements in RC buildings during the L'Aquila, 2009 earthquake. *Bulletin of Earthquake Engineering*, **9** (1), 307-324.

[8] DM (1996): Norme tecniche per le costruzioni in zone sismiche e relative istruzioni. *D.M. 16-01-1996 and C.M. 10-04-1997*, Italian Ministry of Public Works, Rome, Italy.

[9] DM (2018): Norme tecniche per le costruzioni e relative istruzioni. *D.M. 17-01-2018 and C.M. 11-02-2019*, Italian Ministry of the Infrastructures and Transports, Rome, Italy.

[10] Mazza F (2019): In-plane-out-of-plane non-linear model of masonry infills in the seismic analysis of r.c. framed buildings. *Earthquake Engineering & Structural Dynamics*, **48** (4), 432-453.

[11] Mazza F, Donnici A (2019): Effects of in- and out-of-plane nonlinear modelling of masonry infills on the seismic response of r.c. framed buildings. *AIMETA 2019, XXIV Conference of the Italian Association of Theoretical and Applied Mechanics*, Rome, Italy, 2019.

[12] Mazza F, Mazza M (2012): Nonlinear modeling and analysis of r.c. framed buildings located in a near-fault area. *The Open Construction & Building Technology Journal*, **6**, 346-354.

[13] Mazza F, Labernarda R (2018): Effects of nonlinear modelling of the base-isolation system on the seismic analysis of r.c. buildings. *Procedia Structural Integrity*, **11**, 226-233.

[14] Seismosoft (2019): Seismoartif: a computer program for generation of artificial accelerograms. Available from url www.seismosoft.com

[15] Mainstone RJ (1974): Supplementary note on the stiffness and strength of infilled frames. *Current Paper CP 13/74*, Building Research Station, U.K., 1974.

[16] Bertoldi SH, Decanini LD, Gavarini C (1993): Telai tamponati soggetti ad azione sismica, un modello semplificato: confronto sperimentale e numerico. *Proceedings of the VI National Conference on Earthquake Engineering, ANIDIS,* Perugia, Italy.

[17] Dawe JL, Seah CK (1989): Out-of-plane resistance of concrete masonry infilled panels. *Canadian Journal of Civil Engineering*, **16** (6), 854-864.

[18] Kadysiewski S, Mosalam KM (2009): Modeling of unreinforced masonry infill walls considering in-plane and out-of-plane interaction. *Pacific Earthquake Engineering Research Center College of Engineering, University of California, Berkeley*, PEER Report 2008/102.